

U-band photometry of 17 WINGS clusters

A. Omizzolo^{1,2}, G. Fasano², D. Reverte Paya³, C. De Santis^{4,5}, A. Grado⁶, D. Bettoni², B. Poggianti², M.D'Onofrio⁷,
A. Moretti⁷, J. Varela⁸, J. Fritz⁹, M. Gullieuszik², A. Cava¹⁰, A. Grazian¹¹, and M. Moles⁸

¹ Specola Vaticana, 00120 Vatican City State

² INAF- Padova Astronomical Observatory, Vicolo Osservatorio 5, 35122 Padova, Italy

³ GRANTECAN S. A., Centro de Astrofísica de La Palma, C/Cuesta de San José s/n, 38712 Breña Baja (La Palma), Spain

⁴ INFN, Sezione di Roma Tor Vergata, I-00133 Rome, Italy

⁵ Department of Physics, University of Rome Tor Vergata, I-00133 Rome, Italy

⁶ INAF- Napoli Astronomical Observatory, Salita Molariello 16, 80131 Napoli, Italy

⁷ Department of Physics and Astronomy, Vicolo Osservatorio 2, 35122 Padova, Italy

⁸ Centro de Estudios de Física del Cosmos de Aragón (CEFCA), Plaza San Juan 1, planta 2, E-44001 Teruel, Spain

⁹ Sterrekundig Observatorium Vakgroep Fysica en Sterrekunde Universiteit Gent, Krijgslaan 281, S9 9000 Gent

¹⁰ Observatoire de Genève, Université de Genève, 51 Ch. des Maillettes, 1290 Versoix, Switzerland

¹¹ INAF- Roma Astronomical Observatory, I-00040 Monteporzio Italy

Received / Accepted

ABSTRACT

Context. This paper belongs to a series presenting the *Wide Field Nearby Galaxy-cluster Survey* (WINGS). The WINGS project has collected wide-field, optical (B,V) and near-infrared (J,K) imaging, as well as medium resolution spectroscopy of galaxies in a sample of 76 X-ray selected nearby clusters ($0.04 < z < 0.07$), with the aim of establishing a reference sample for evolutionary studies of galaxies and galaxy clusters.

Aims. In this paper we present the U-band photometry of galaxies and stars in the fields of 17 clusters of the WINGS sample. We also extend to a larger field of view the original B- and V-band photometry (WINGS-OPT) for 9 and 6 WINGS clusters, respectively.

Methods. We use both the new and the already existing B-band photometry to get reliable (U-B) colors of galaxies within three fixed apertures in kpc. To this aim, in the reduction procedure we put particular care in the astrometric precision. Since not all the observations have been taken in good transparency conditions, the photometric calibration was partly obtained relying on the SDSS and WINGS-OPT photometry for the U- and optical bands, respectively.

Results. We provide U-band (also B- and V-band, where possible) total magnitudes of stars and galaxies in the fields of clusters. Just for galaxies, the catalogs also provide geometrical parameters and carefully centered aperture magnitudes. The internal consistency of magnitudes has been checked for clusters imaged with different cameras, while the external photometric consistency has been obtained comparing with the WINGS-OPT and SDSS surveys.

Conclusions. The photometric catalogs presented here add the U-band information to the WINGS database for extending the SED of the galaxies, in particular in the UV wavelengths which are fundamental for deriving the SFR properties.

Key words. Galaxies: clusters: photometry

1. Introduction

In the currently standard cosmological paradigm, clusters accrete individual galaxies and larger subclumps from their outskirts. In this scenario, the infalling regions of clusters are naturally very important, being the transition regions in which galaxies are subject to a dramatic change of environment, feeling the effects of the high density environment for the first time. A morphological transformation of spirals into S0 galaxies appears to occur in clusters at $z > 0.2$, most likely driven by environmental effects (Dressler et al. 1997, Fasano et al. 2000). The environment also appears to have a strong influence on the star formation activity of disk galaxies in clusters at high redshift, apparently suppressing it upon infall into rich clusters (Balogh et al. 1997; Couch et al. 1998, 2001; Dressler et al. 1999; Poggianti et al. 1999). Indeed, observations probing the star formation, Hubble types and gas content of galaxies in clusters have proved that the cluster outskirts are essential to understand galaxy transformations

(Abraham et al. 1996; Balogh et al. 1997; Ellingson et al. 2001; Solanes et al. 2001; Pimbblet et al. 2002; Treu et al. 2003; Kodama et al. 2001; Kodama et al. 2004; McIntosh et al. 2004). In particular, several recent works have shown that in the local Universe the correlation between star formation activity and local density extends to very large clustercentric radii, well beyond the cluster central regions (Lewis et al. 2002; Gomez et al. 2003; Balogh et al. 1997). The assembly of clusters, by itself, seems to be able to suppress the star formation, as suggested by the detection of post-starburst galaxies at the interface of cluster infalling substructures (Poggianti et al. 2004).

In the last years many high quality (HST) observations have been devoted to the study of clusters at intermediate and high redshift, while for the local volume, till a few years ago, Virgo, Fornax and Coma clusters constituted the main reference sample. To fill in this gap, we started the *Wide Field Nearby Galaxy-cluster Survey* (WINGS Fasano et al. 2006, hereafter Paper-I). This survey has focused on clusters located in the redshift range $0.04 - 0.07$ and has collected

Send offprint requests to: alessandro.omizzolo@oapd.inaf.it

wide-field optical (B,V) imaging (Varela et al. 2009, WINGS-OPT) for a sample of 76 clusters selected from three X-ray flux limited samples compiled from ROSAT All-Sky Survey (Ebeling et al. 1996; Ebeling et al. 1998; Ebeling et al. 2000). In addition, multi-fiber, medium resolution spectroscopy and near-infrared (J,K), wide-field imaging have been obtained for 48 and 28 WINGS clusters, respectively (Cava et al. 2009; Valentinuzzi et al. 2009).

To complement the WINGS database with U-band imaging, we have gathered observations for a subsample of 17 WINGS clusters using three different telescopes equipped with different wide-field cameras and a few archival data.

These observations will allow to study in detail the star formation activity in a statistically significant sample of cluster galaxies. As the integrated spectrum of a galaxy is more and more dominated by young stars going to shorter wavelengths, U-band data is by far more sensitive to any current or recent star formation than any of the other broad-bands available (Kennicutt 1998; Barbaro & Poggianti 1997). Our U-band estimates of the current star formation are truly integrated values (though dust-affected), to be compared with the estimates based on our optical spectroscopy, which samples only the very central regions of each galaxy ($1.6''/2.6''$). Moreover, the spatial distribution of the U-band emission within galaxies greatly helps to discriminate between the various physical processes, by revealing if star formation preferentially is suppressed and/or enhanced in the central and outskirts regions of galaxies. In particular, the distribution of the star formation activity (SFA) in galaxies residing in the cluster outskirts (infalling region) could reveal if they are affected by ram pressure stripping (SFA in the outer regions), by shock-induced star formation related to the galaxy infalling into the cluster (SFA on the impact edge of the galaxies), or by centrally driven starbursts due to tidal repeated encounters in the cluster potential (SFA in the nuclear regions). Moreover, these observations should allow us to establish how the SFA correlates with galaxy morphology (from the V-band imaging), mass (from K-band data) and spectra, as well as with the environment (local density and cluster properties).

The paper is organized as follows. Section 2 describes our observations and data reduction. In Section 3 we present the catalogs and in Section 4 the data quality is analyzed. Through the paper we use the following cosmology: $H_0 = 70 \text{ km s}^{-1} \text{ Mpc}^{-1}$, $\Omega_m = 0.3$ and $\Omega_\Lambda = 0.7$. The magnitudes are in the Vega system.

2. Observations and data reduction

The data presented in this paper are based on observations obtained with three different wide-field cameras (see Table 1): (i) the 90prime camera at the 90 inches BOK telescope (90prime@BOK, Kitt Peak); (ii) the Wide Field Camera at the 2.5m Isaac Newton Telescope (WFC@INT); (iii) the Large Binocular Camera at the Large Binocular Telescope (LBC@LBT). For one cluster (Abell 970) we used imaging data from the WFI@MPG (ESO2.2 archive). All clusters have been imaged in the U-band. Many clusters have also been imaged in the optical (B,V) bands.

In Table 2 we report the observing log, one row per run (per night in the case of the LBC observations), each row including the number of imaged clusters. In Table 3 the list of the observed clusters is reported. Besides the average coordinates and redshifts of the clusters, in column 5 we list the telescopes used to image each cluster. The BOK observations always include the U-, B- and V-bands, while the INT and MPG observations just include the U-band. For the clusters imaged with LBT, we list

Telescope (Camera)	Pixel scale	e^-/ADU	RON e^-	FOV
INT (WFC)	0.333''	2.8	6.2	34'x34'
BOK (90prime)	0.450''	1.71	12	90'x90'
LBT (LBC)	0.226''	2.022	11.45	23.6'x25.3'
MPG (WFI)	0.238''	2.0	4.5	34'x33'

Table 1. The cameras.

Date	Telescope	N
February 27-29 2000	WFI@MPG	1
May 10-14 2005	WFC@INT	8
June 20-22 2006	90prime@BOK	2
November 22-23 2006	90prime@BOK	4
March 12 2007	LBC@LBT	1
May 19 2007	LBC@LBT	1
June 04 2008	LBC@LBT	2
June 07 2008	LBC@LBT	1
June 08 2008	LBC@LBT	2

Table 2. The runs. For each run: (1) the date; (2) the name of the telescope; (3) number N of clusters observed.

ID	$\alpha J2000$	$\delta J2000$	z	Telescope
A0119	00 56 21	-01 15	0.0444	BOK
A0970	10 17 34	-10 42	0.0580	MPG
A1291	11 32 21	55 58	0.0527	INT
A1668	13 03 46	19 16	0.0634	LBT (U)
A1795	13 48 52	26 35	0.0622	BOK, INT, LBT (U,B)
A1831	13 59 15	27 58	0.0612	INT
A1983	14 52 59	16 42	0.0444	INT
A1991	14 54 31	18 38	0.0586	LBT (U,B)
A2107	15 39 39	21 46	0.0411	BOK, LBT (U,B)
A2124	15 44 59	36 06	0.0654	INT, LBT (U,B)
A2149	16 01 35	53 55	0.0675	BOK
A2169	16 14 09	49 09	0.0579	INT
A2399	21 57 13	-07 50	0.0582	BOK
RXJ1022	10 22 10	38 31	0.0534	BOK
RXJ1740	17 40 31	35 39	0.0430	LBT(B)
ZwCl2844	10 02 36	32 42	0.0500	INT
ZwCl8338	18 10 50	49 55	0.0473	INT

Table 3. The observed clusters.

in parenthesis the filters used for the imaging. The *FWHMs* for each cluster in each filter are given in the headers of the catalogs (see in Figure 1 the first group of rows of the header). With the WFC, 90prime and LBC cameras we have imaged 8, 6 and 6 clusters, respectively. Some clusters have been observed with two or three instruments for a total of 15 clusters observed in the U band. To these observations we added U-band imaging of the cluster Abell 970, taken from the WFI@MPG (ESO2.2 archive). The data sets coming from the four instruments (WFC, 90prime, LBC and WFI) span a time interval of about four years and reflect different proposal strategies (observing constraints and requirements), also depending on the available observing time. Therefore, because of the quite heterogeneous instrument sets and weather conditions, we used different reduction strategies for the different cameras, as outlined in the following subsections.

2.1. INT observations

We obtained WFC@INT imaging of 9 clusters during three useful nights of the same observing run (May 10/12/13 2005). For the outline of the camera we refer to Table 1 and Paper-I. The ob-

servations have been taken, under generally good weather conditions, just in the U-band and trying to match as much as possible the field of view of the B- and V-band imaging already available in the WINGS-OPT survey. To cover the gaps between the CCDs, at least three 20 min dithered exposures per cluster have been done. During each night standard field exposures have been secured to allow the photometric calibration.

Bias subtraction and flat-field corrections were separately performed on each of the four CCDs of the WFC, while the mosaic-image of each exposure was produced using the IRAF tool `wfcmosaic`. The mean error of the astrometric solution, obtained for every exposure through the USNO star catalog, turned out to be ≤ 0.3 arcsec (~ 1 pixel) over the field. The final image of each cluster was obtained by weighted mean combination of the dithered exposures.

During the run, the system proved to be rather stable, while the photometric calibration showed that the transparency did not change significantly. The cluster A1991 was excluded from the final INT sample since the outlined reduction procedure was not able to repair some temporary failure of the acquisition system causing a lack of homogeneity among the CCDs.

2.2. BOK observations

The 90prime camera mounted at the BOK telescope (Kitt Peak) during our 2006 observing runs was a mosaic of four CCDs separated in both directions by very large inter-CCD gaps (about 15.76 mm or 1050 pixels). The edge-to-edge field of view, including the inter-CCD gaps, was 1.16×1.16 degrees, with a plate scale of $30.2''/\text{mm}$ or $0.45''/\text{pixel}$.

In five nights, sharing two observing runs (see Table 2 for details), we have imaged 8 clusters in the U-, B- and V-band. In order to fill the large gaps between the CCDs, we shifted the telescope in 5 different positions, thus covering the entire field of view of the camera.

During each night, dome and twilight sky flats were obtained and several photometric standard fields were imaged in each photometric band and at different zenithal distances. Unfortunately, in both observing runs the weather conditions were inclement. In particular, the average seeing was about $2''$ and the sky transparency was not good.

Due to the very large angular view provided by the 90prime camera, in order to obtain a good enough astrometry over the whole field, we were forced to adopt a more laborious procedure with respect to the INT data reduction. In particular, relying on the stars of the USNO catalog in a suitable (filter dependent) magnitude range, we first obtained, for each filter and for each CCD, an average astrometric solution relative to the geometrical center of the camera, staking altogether the mosaic images obtained in that filter. Then, using 15 stars for each CCD (3 in every corner and 3 in the center), we improved the astrometric solution of each CCD for each exposition and translated it into the proper position on the sky. The *rms* of the angular distances between the BOK and USNO coordinates turned out to be less than 0.25 arcseconds.

To obtain the final mosaic for every field, we used SWARP (Bertin & Arnouts 1996) by `Terapix`. Using our astrometric projection defined in the WCS standard, for each cluster in each filter, SWARP resampled and co-added the set of five dithered exposures, thus producing the final, background-subtracted image. Two of the eight imaged clusters (A2256 and RX0058) were observed under quite poor weather conditions. They have not been included in the final BOK sample.

Even though the standard field exposures were diligently processed as we did for the scientific ones, they were just used to obtain the relative photometric calibration within the 90prime field, i.e. to estimate possible gain and linearity differences among the CCDs. In fact, because of the poor transparency, we were forced in both runs to perform the absolute photometric calibration (zero points and color terms) relying on the WINGS-OPT catalogs (Varela et al. 2009, for the V- and B-band) and on the Sloan Digital Sky Survey DR7 photometric data (Abazajian et al. 2008), suitably converted to the Johnson system (Lupton 2005, for the U-band).

2.3. LBT observations

LBC fits images are Multi Extension Files (MEF) composed by a mosaic of 4 CCDs of 4608×2048 pixels with a median plate scale of $0.225''/\text{pixels}$ and a scientific field of view (FoV) of about 23.6×25.3 arcmin². Therefore, in order to cover the field imaged by the WINGS-OPT survey, five exposures per cluster were planned.

The observations of our clusters have been taken in service mode, during the Science Demonstration Time (SDT) under variable transparency and seeing conditions. The data set resulting from these circumstances was not optimal, since in many cases the cluster field coverage was incomplete (sometimes sparse), or the different exposures of the same cluster were taken in different seeing and transparency conditions. At the end, just 6 clusters turned out to have enough field coverage and seeing homogeneity to be included in the final LBT sample. Three of them were imaged in both U- and B-band, while for two clusters just the U-band imaging was available. Finally, for RX1740 we just obtained B-band imaging.

The reduction has been performed by one of us (CD) using the standard procedure devised by the LBC Team¹. In most CCD mosaic imagers, electronic ghosts are present due to video channel's cross-talk and a specifically designed software procedure (`xtalk`) has been used to remove these features; for LBC the cross talk coefficient is about $3.0E-05$.

The flat field images were derived from twilight sky data and a calibration master flat was obtained by stacking a set of flat images with a sigma clipping rejection algorithm with radial profile normalized to unity in the center. The saturated pixels, chips' bad signatures, cosmic ray events and satellite trails were masked using a special derivative algorithms developed by the LBC Team.

The area of the LBC pixels is not constant over the entire FoV, due to the effect of astrometric distortions (also called sky concentration). To correct this feature and normalize the pixel area, a sky-concentration image was applied as multiplicative factor. This filter dependent correction image was produced by a specific software that uses as input information the astrometric solution for the specific filter. After this correction, it was possible to mask all objects in the image and stack all frames within a fixed temporal window (about 10 minutes), in order to allow a proper subtraction of the small scale features of the background. This temporal window is representative of the main sky background variation and features such as fringes. For the U- and B-band this procedure produced well flattened images and no further processing was required.

The background subtracted images were corrected for object photometry altered by sky-concentration effects dividing for the same correction image used in the previous reduction step. In fact, the sky concentration effects modify the surface bright-

¹ <http://lbc.oa-roma.inaf.it/>

ness of the background, producing a typical pin-cushion feature, but it does not alter the integrated flux of extended objects. Therefore, each science image must first be multiplied by the sky-concentration image to rectify the background, and once it is properly subtracted, it must be divided by the same sky-concentration image to correct the flux of stars and galaxies to their original value. Being a prime focus camera, the optical distortions of LBC are quite relevant. Still, after the above outlined procedure, the quality of the PSF over the entire LBC FoV turned out not to depend on the radial distance from the optical center.

The astrometric solution was computed through a three-pass process by the AstromC package (Radovich et al. 2004): 1) the offset of the four chips were computed by matching a catalog of objects found on the frame with an astrometric catalog (usually USNOA B1.0 catalog); 2) an overall fit was performed to obtain a local chip-to-chip astrometric solution applying the calculated deformation map obtained with Stone (1997) astrometric fields (and UCAC catalogs), as described in Giallongo et al. (2008, G08 hereafter); 3) the final astrometric solution was computed on the whole dithered image set thus providing a well minimized global fit.

Since no photometric standard fields were imaged during the SDT runs, the (provisional) photometric calibration was obtained using the coefficients given in Table 2 of G08. These coefficients are the result of several commissioning nights just devoted to the photometric characterization of LBC@LBT. The nominal photometric accuracy in the overall field is of the order of 0.01 mags. We refer to G08 for further details about the LBC instrument and the data reduction procedures. The final zero points have been checked (and sometime improved) using the SDSS DR7 and the WINGS-OPT databases for the U- and B-band, respectively.

2.4. ESO WFI@MPG archival data

From the ESO archive we retrieved U-band deep observations of one more cluster, namely A970. The images were taken during the night of Feb. 28, 2000. They have been processed using the VST-Tube (Grado et al. 2010) pipeline. In particular, after bias and flat-field correction, to the mosaic image a provisional absolute calibration was applied using a few photometric standard field observed during the same night and adopting the extinction coefficient given in the ESO La Silla WEB page (0.48).

The same photometric standard fields were used to determine the illumination correction map. This has been obtained by using a generalized adaptive method (GAM) to interpolate the difference between raw and standard magnitudes as a function of the position. The GAM allows to obtain a well behaved surface also in case (like the present one) the field of view is not uniformly sampled by the standard stars. The illumination map image was then used to correct the science images during the pre-reduction stage. After applying the illumination correction the (raw - standard) magnitude difference is reduced by a factor ~ 2 .

The gain harmonization among the CCDs and the astrometric solution were obtained using SCAMP (Bertin 2007). The r.m.s. (along each axis) of the pairwise differences between coordinates of overlapping detections and between detection coordinates and coordinates of the associated astrometric reference stars, turned out to be 0.177" and 0.168", respectively.

Columns 2 and 3 of Table 4 list the median seeing (*rms* in parenthesis) and the astrometric quality of the final mosaics for each camera.

3. The Catalogs

The source detection and extraction has been performed using SExtractor (Bertin & Arnouts 1996, SEx hereafter). For each mosaic frame, with the proper seeing and photometric depth, we performed a number of test runs of SEx to identify the most suitable values of the deblending parameters, trying to find compromise values running well for different kinds of objects. In this way, we sacrificed the homogeneity of the catalogs in order to obtain galaxy samples as complete as possible. For each telescope (INT/BOK/LBT/ESO) we provide catalogs of each cluster, including the magnitudes for all the available photometric bands. SExtractor provided integrated (MAG_AUTO) magnitudes of sources, as well as the geometrical parameters of galaxies and the automatic star/galaxy classifier. Where possible, the geometrical and star/galaxy SEx parameters are referred to the B-band. In case the B-band imaging is not available, they are referred to the U-band imaging.

In the original, WINGS-OPT catalogs, particular care was devoted to distinguish stars and galaxies (see Section 2.3 in Varela et al. 2009). Therefore, we assumed that the star/galaxy classification given therein is correct and, in each cluster, we adopt this classification for the objects in common with the WINGS-OPT catalogs. Moreover, the common objects have been used to compare the continuous (from 0 to 1) star/galaxy SEx classifier of the new catalogs with the binary star/galaxy classifier of the old WINGS-OPT catalogs. In particular, using the star/galaxy, ellipticity and FWHM parameters of the new SEx catalogs, for each camera of the present survey, we have identified some empirical criteria to *transfer* the old classification to the objects not in common with WINGS-OPT. We adopt this second-hand, indirect (binary) classification for the 'new' objects, which mostly reside in the outer cluster regions, not sampled by the original WINGS-OPT survey. From the visual check of 200 detections (100 stars and 100 galaxies), randomly selected among the 'new' objects of all catalogs with magnitude $U_{Tot} < 22.5$, it turned out that this indirect, binary classification is correct for 83 and 75 stars and galaxies, respectively, while for 28 objects the visual classification is uncertain. The percentages become higher (44/45 and 17/18 for stars and galaxies) if one considers just objects with $U_{Tot} < 20.5$.

In spite of the relatively high values chosen for the detection threshold ($1.5\sigma_{bkg}/pixel$), the number of detected sources in each filter turned out to be often quite large, due to the large number of spurious detections. Therefore, where possible (i.e. for clusters observed in two or three bands), we decided to retain in the final catalogs just the sources detected in all the available photometric bands, thus producing catalogs which include, for the common objects, the total magnitudes SExtracted in the different bands.

As mentioned in the previous section, while for the INT and ESO imaging the photometry can rely on their own absolute calibrations, for the BOK and LBT imaging the absolute calibration has been obtained relying on the SDSS and WINGS-OPT star magnitudes for the U-band and for the optical (B,V) bands, respectively. When two or three bands were available for a given cluster, this relative calibration also takes into account the color terms derived from the provisional SEx magnitudes. The comparison U-band magnitudes are obtained from the *u, g, r* SDSS (DR7) magnitudes, using the conversion formula by Lupton (2005).

Perhaps the most important target for the U-band photometry of large galaxy samples in clusters is to determine their colors. It is well known that, in order to obtain reliable color estimates, it is crucial to measure the magnitudes inside apertures

Telescope (Camera)	FWHM	Astrometry	$U_{lim}(90\%)$	$B_{lim}(90\%)$	$V_{lim}(90\%)$
INT (WFC)	1".30 (0".27)	<0".3	22.3÷23.3		
BOK (90prime)	1".93 (0".23)	<0".25	21.3÷22.1	21.1÷22.6	20.0÷22.5
LBT (LBC)	1".40 (0".24)	<0".22	22.6÷23.3	23.1÷23.6	
MPG (WFI)	0".9	<0".19	22.1		

Table 4. Quality of observations

```

#
# A1795 BOK imaging (zPs corrected for comparison with WINGS and SDSS)
#
# FWHM (U-band)=1.85
# FWHM (B-band)=2.03
# FWHM (V-band)=1.68
#
# 90% compl.(U-band)=22.1
# 90% compl.(B-band)=22.6
# 90% compl.(V-band)=21.5
#
# <U_BOK-U_SDSS>(Tot)=-0.102
# <B_BOK-B_WINGS>(Tot)=-0.008
# <B_BOK-B_WINGS>(2kpc)=0.332
# <B_BOK-B_WINGS>(5kpc)=0.074
# <B_BOK-B_WINGS>(10kpc)=-0.013
# <V_BOK-V_WINGS>(Tot)=-0.038
# <V_BOK-V_WINGS>(2kpc)=0.264
# <V_BOK-V_WINGS>(5kpc)=0.080
# <V_BOK-V_WINGS>(10kpc)=-0.018
#
# rms(U)=10**((0.2-0.342*U+0.0141*U*U)
# rms(B)=10**((0.4-0.33*B+0.0118*B*B)
# rms(V)=10**((0.86-0.255*V+0.0081*V*V)
#
#
# 1 WINGS_ID
# 2 ALPHA_SKY Right ascension of barycenter (sky) [deg]
# 3 DELTA_SKY Declination of barycenter (sky) [deg]
# 4 WINGS_classification: Star/Galaxies/Unknown (2/1/0)
# 5 ISORHSA_IMAGE B-band isophotal area above Analysis threshold [pixel**2]
# 6 KRON_RADIUS B-band Kron apertures in units of A
# 7 A_IMAGE B-band Profile RMS along major axis [pixel]
# 8 B_IMAGE B-band Profile RMS along minor axis [pixel]
# 9 THETA_IMAGE B-band Position angle (CCW/x) [deg]
# 10 MAG_AUTO (U-band)
# 11 MAG_APER_2KPC (U-band)
# 12 MAG_APER_5KPC (U-band)
# 13 MAG_APER_10KPC (U-band)
# 14 MAG_AUTO (B-band)
# 15 MAG_APER_2KPC (B-band)
# 16 MAG_APER_5KPC (B-band)
# 17 MAG_APER_10KPC (B-band)
# 18 MAG_AUTO (V-band)
# 19 MAG_APER_2KPC (V-band)
# 20 MAG_APER_5KPC (V-band)
# 21 MAG_APER_10KPC (V-band)
# 22 APERTURE_FLAG 0=free
#
# 1=centered on WINGS_OPT (just galaxies in common with WINGS)
# 2=centered on BOK B-band (just galaxies not in common with WINGS)
#
#
# WINGS_ID      ALPH      DELT  SGU  BAREA  BKRONR  BAMAJ  BAMIN  BPA    UC    UC2   UC5   UC10  BC    BC2   BC5   BC10  VC    VC2   VC5   VC10  AFLAG
#
# WINGSJ134725.85+263756.7  206.85786  26.63246  1  190  4.3  4.119  2.685  -47.9  20.49  21.6  20.71  20.63  20.58  21.71  20.73  20.38  21.37  -99.0  -99.0  -99.0  2
# WINGSJ134726.17+263310.8  206.85869  26.55304  1  56  5.2  2.332  1.648  -20.1  22.64  22.98  22.63  22.81  22.01  22.69  21.69  20.77  -99.0  -99.0  -99.0  2
# WINGSJ134726.17+264019.4  206.85925  26.672  1  49  5.1  2.094  1.696  33.9  21.97  22.46  21.95  21.89  22.48  22.85  22.3  21.81  21.33  21.85  21.66  -99.0  2
# WINGSJ134726.19+265932.4  206.85903  26.99243  1  55  4.0  2.295  1.733  -17.2  21.48  22.16  21.53  21.78  22.19  22.8  22.2  22.01  21.62  22.42  21.78  21.42  2
# WINGSJ134726.21+263527.5  206.85921  26.59102  0  98  3.9  2.697  2.138  -3.9  21.18  21.76  21.12  21.06  21.18  21.74  21.18  21.08  19.95  20.39  19.94  20.04  0
# WINGSJ134726.28+263304.9  206.85944  26.55141  0  8  7.8  0.892  0.681  51.3  23.15  23.14  23.4  22.73  23.45  23.87  23.58  23.68  22.41  22.86  22.37  22.3  0

```

Fig. 1. Header and first rows of the catalog from BOK imaging of A1795

centered exactly at the same points in the two bands. On the other hand, since galaxies (especially of late-type morphology) may look differently in different bands, the geometrical centers coming from automatic SExtraction of sources turn out to be usually different in the different bands. To overcome this problem, we have used a purposely devised script, based on the IRAF `apphot` package, allowing us to measure the aperture magnitudes exactly on the requested positions, with the requested radii. Since in the WINGS-OPT catalogs we report the aperture magnitudes within circular apertures of radii 2, 5 and 10 kpc, for all galaxies in common with WINGS-OPT we measured the aperture magnitudes in the U-band (and also in the optical bands, where possible) adopting exactly the same centers and radii of the WINGS-OPT survey. In the catalogs we report a special Aperture Flag (AFLAG, see Figure 1: last column), that for galaxies in common with WINGS-OPT is set to 1. If the cluster has been imaged with some camera in both the U- and B-band, we centered the U-band aperture magnitudes of the galaxies not in common with WINGS-OPT on the apertures given by SEx for the B-band imaging. For these galaxies AFLAG is set to 2 in the catalogs. In the remaining cases (all stars and those galaxies not in common with WINGS-OPT and just imaged in the U-band) AFLAG is set to zero.

As an example of the catalogs presented in this paper, Figure 1 shows the header and the first rows of the catalog from the BOK imaging of A1795. The *rms* of magnitudes as a function of the magnitudes themselves have been estimated fitting

band	U (<20.5)			B (<20.5)
	BOK-INT	BOK-LBT	LBT-INT	BOK-LBT
Total	-0.01 (0.06)	0.00 (0.10)	0.01 (0.07)	-0.03 (0.06)
2kpc	0.00 (0.07)	0.09 (0.09)	-0.09 (0.06)	0.13 (0.07)
5kpc	0.00 (0.04)	0.02 (0.06)	0.00 (0.04)	0.00 (0.07)
10kpc	-0.03 (0.08)	0.01 (0.14)	0.00 (0.09)	-0.03 (0.08)

Table 5. Median values and *rms* (in parenthesis) of the magnitude differences for internal comparisons

second order polynomials to the decimal logarithm of the magnitude binned *rms* of the differences between the total magnitudes of galaxies and the comparison magnitudes from the WINGS and/or SDSS surveys. These polynomials are reported in the headers of catalogs (see Figure 1: fourth group of rows in the header) and can be used to assign individual errors to the magnitudes.

4. Data quality

4.1. Internal comparisons

In Figure 2 we show the differences between magnitudes obtained using different cameras for common objects (black and red dots for galaxies and stars, respectively) as a function of the magnitude of one of the two cameras, usually the one providing

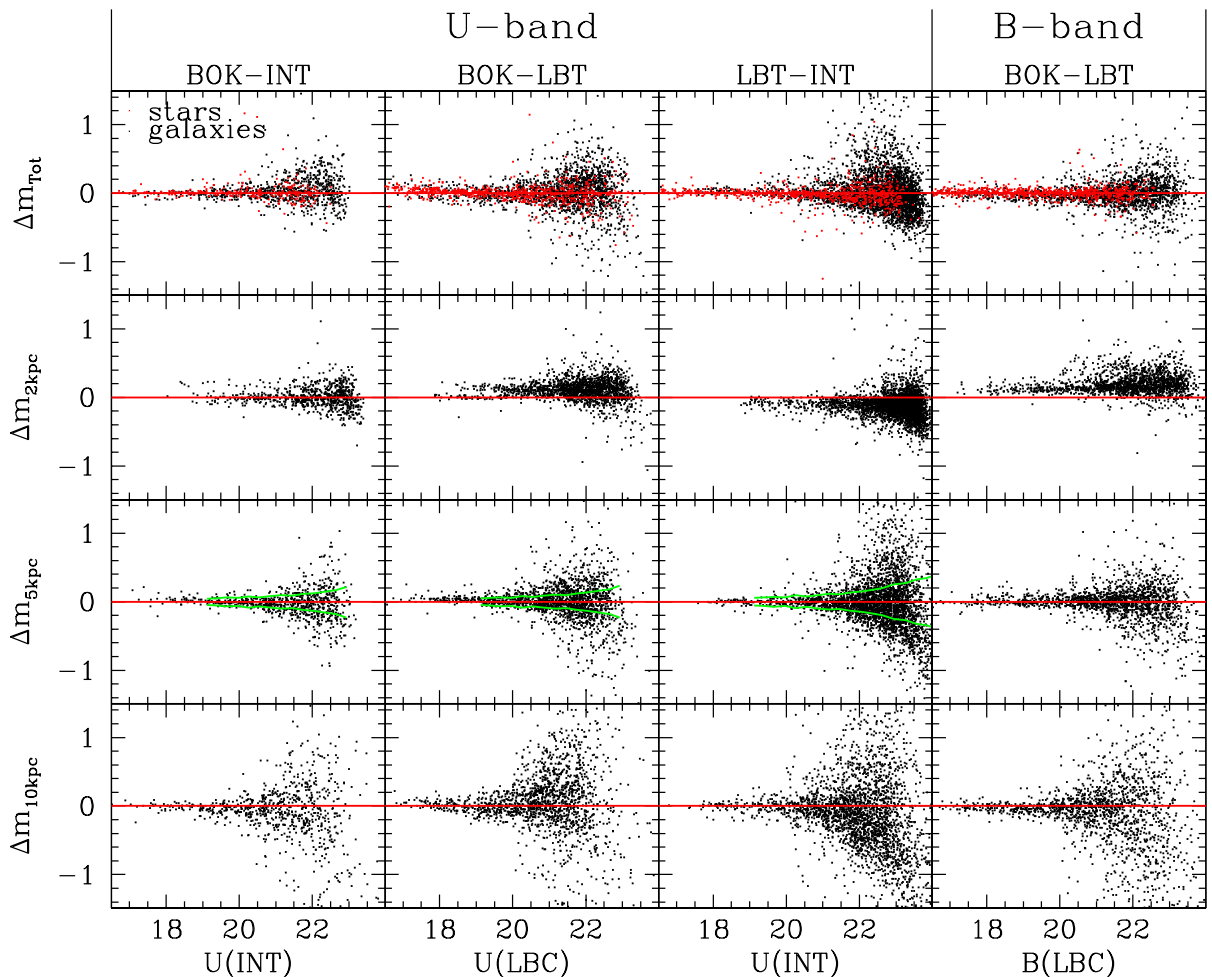


Fig. 2. Differences between magnitudes obtained using different cameras for common galaxies (black dots) as a function of the magnitude. The plots in the topmost row of the figure refer to the total magnitudes, while those in the remaining rows refer to the magnitudes within circular apertures of radii 2, 5 and 10 kpc, top to down. The plots in the rightmost column of the figure refer to the B-band, while those in the other columns refer to the U-band. The red dots in the plots of the topmost row of the figure (total magnitudes) refer to the stars. The green curves in the plots relative to the 5 kpc apertures (third row of the figure) illustrate the *rms* expected according to the formulas reported in the headers of the catalogs (see text for details).

the most reliable values. The green curves in the plots relative to the 5 kpc apertures (third row of the figure) illustrate the *rms* expected according to the formulas reported in the headers of the catalogs (see last sentence of Sec. 3) as a function of the magnitude. In particular, for each couple of cameras to be compared, the *rms* (green) curve is obtained using the error propagation rules to combine the *rms* formulas (reported in the catalog header) of the common clusters for both cameras and weighting each *rms* formula according to the number of galaxies in the relative catalog. A quick report of the photometric agreement among the INT, BOK and LBT cameras for galaxies in common clusters is given in Table 5. Here, for each magnitude (Total, 2 kpc, 5 kpc and 10 kpc) and for each pairwise comparison, we list the median value and the *rms* (in parenthesis) of the magnitude differences up to a given total apparent magnitude (19.5, in both the B- and U-band).

From Figure 2 and Table 5, the agreement among the U-band magnitudes of the different cameras turns out to be generally good, although for the median values this comparison test is actually meaningful just for the INT magnitudes, since both the BOK and LBT magnitudes have been calibrated on the SDSS

magnitudes. The same holds for the BOK-LBT comparison of the B-band magnitudes (plots in the rightmost column of the figure). In fact, since the BOK and LBT B-band magnitudes have been both calibrated on the WINGS optical survey, again this comparison just provides a consistency test.

From Figure 2, the only remarkable (and systematic) disagreement among the cameras concerns the magnitudes within circular apertures of radius 2 kpc. In this case the average differences reflect both the different average seeing conditions relative to the different cameras and the peculiar seeing of the mosaic image of each cluster. The influence of the seeing already disappears in the case of the circular apertures of radius 5 kpc, for which also the scatter in the plots turns out to be in reasonably fair agreement with the expected *rms* (green curves) and better than in the case of 10 kpc aperture magnitudes.

4.2. External comparisons

Figure 3 is similar to Figure 2, but illustrates the quality of B- and V-band photometry through a comparison between the mag-

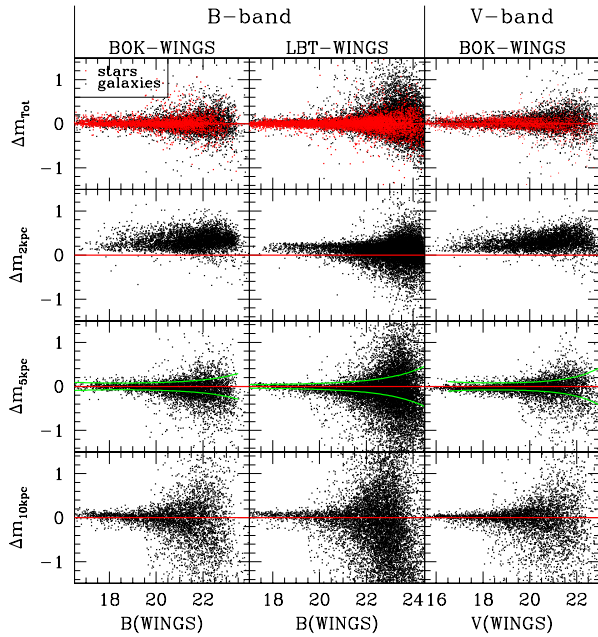


Fig. 3. Differences between optical bands (B,V) magnitudes from the catalogs presented here and the corresponding magnitudes in the original WINGS optical survey as a function of the WINGS magnitudes for the galaxies in common (black dots). The plots in the topmost row of the figure refer to the total magnitudes, while those in the remaining rows refer to the magnitudes within circular apertures of radii 2, 5 and 10 kpc, top to down. The plots in the rightmost column of the figure refer to the V-band, while those in the other columns refer to the B-band. The red dots in the plots of the topmost row of the figure (total magnitudes) and the green curves in the plots relative to the 5 kpc apertures (third row of the figure) are as in Figure 2

band	B (<20.5)		V (<19.5)
	BOK-WINGS	LBT-WINGS	BOK-WINGS
Total	-0.01 (0.08)	0.03 (0.06)	0.02 (0.07)
2kpc	0.27 (0.14)	0.16 (0.09)	0.21 (0.12)
5kpc	0.08 (0.07)	0.07 (0.07)	0.06 (0.05)
10kpc	0.01 (0.13)	0.03 (0.14)	0.00 (0.10)

band	U (<20.5)		
	INT-DSS	BOK-SDSS	LBT-SDSS
Total	-0.05 (0.17)	0.00 (0.20)	-0.01 (0.19)

Table 6. Median values and *rms* (in parenthesis) of the magnitude differences for external comparisons

nitudes listed in the catalogs presented here and the corresponding magnitudes from the WINGS optical survey. It is worth recalling that, since the BOK and LBT optical magnitudes have been both calibrated on the WINGS optical survey, this comparison just provides an estimate of the photometric quality (scatter) of the BOK and LBT data as a function of the WINGS magnitudes.

For Figure 3 one could repeat the same considerations of the previous subsection (Figure 2) as far as both the systematic disagreement of the magnitudes within circular apertures of radius

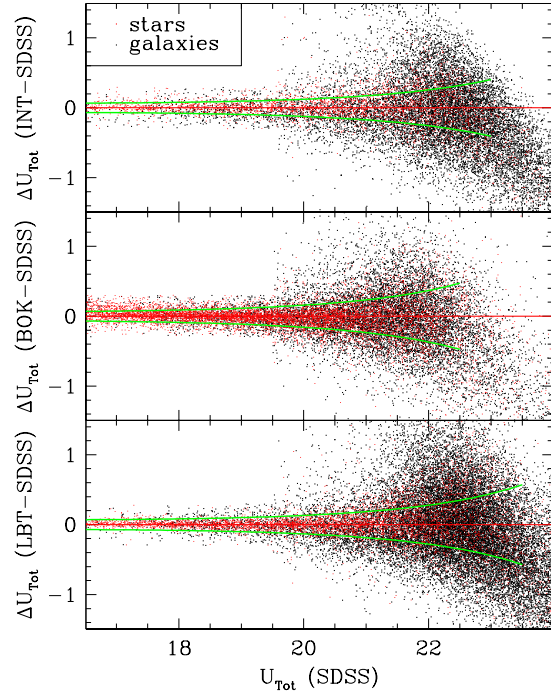


Fig. 4. Differences between U-band total magnitudes from the catalogs presented here and the corresponding magnitudes derived from the SDSS magnitudes using the conversion formula by (Lupton 2005) as a function of the SDSS magnitudes. Black and red dots in the plots refer to galaxies and stars, respectively.

2 kpc and the expected *rms* as a function of the magnitude (green curves in the 5 kpc aperture magnitudes plots).

In Figure 4 the U-band magnitudes of the present survey are compared with the corresponding U-band magnitudes derived from the SDSS database using the formula provided by Lupton (2005). Again, since the BOK and LBT U-band magnitudes have been both calibrated on the SDSS data, the middle and bottom panels of the figure just provide an estimate of the photometric quality (scatter) of the BOK and LBT magnitudes as a function of the SDSS data. Instead, the uppermost plot in the figure illustrates the fair agreement between the SDSS and INT U-band photometric zero-points. Table 6 is similar to Table 5, but refers to the external comparisons. In this case the limiting magnitudes adopted to compute the median values and the *rms* of the magnitude differences are 19.5 for the B- and U-band, while for the V-band we adopt $V_{lim}=20.5$. Note that for the U-band comparisons we just can use the total magnitudes.

Although Table 6 and Figures 3 and 4 refer to all clusters available for the different comparisons, we recorded the average magnitude differences for each individual cluster and for each magnitude (total and aperture magnitudes). These average differences are reported in the third group of rows of the header of each catalog (see Figure 1). They could be useful to make the catalog magnitudes (both total and aperture magnitudes) statistically consistent with the WINGS-OPT and SDSS magnitudes, thus allowing a more correct computation of galaxy colors (in particular, aperture colors) for each individual cluster. It is worth remarking, however, that significant differences between

the catalog and comparison (WINGS-OPT and SDSS) magnitudes could persist, depending on the sizes and luminosity profiles of individual galaxies.

4.3. Photometric depth

We used simulations to estimate the detection rate in the different bands as a function of the magnitude. In particular, for each field, we used the IRAF task `mkobj` with the true image PSF to produce a large number of artificial stars and randomly distributed upon the field. In particular, the artificial galaxies were simulated trying to reproduce the magnitude, size and ellipticity distributions of the galaxies in the real image. Most artificial objects were simulated in the range of faint magnitudes, where SEx is less reliable. The artificial objects were added to the original frames and, on the new images, SEx was run using the same configuration files used to derive the original catalogs. The resulting catalogs were matched with the catalogs of the artificial objects and the fraction of them recovered by SEx in each magnitude bin was recorded. Figure 5 illustrates the fractions of simulated galaxies retrieved by this procedure as a function of the U-band total magnitudes for the four cameras. Columns 4, 5 and 6 of Table 4 list, for each camera and filter, the range of 90% detection rates of artificial galaxies. Moreover, the second group of rows in the headers of the catalogs (see Figure 1) report the 90% detection rates of artificial galaxies for each band, cluster and telescope. For simulated galaxies, the 90% detection rate in the U-band is reached at different magnitudes for different telescopes and clusters, spanning the intervals (22.30-23.30), (22.60-23.30) and (21.30-22.10) for the INT, LBT and BOK imaging, respectively. The INT and LBT telescopes provided similar results, both in terms of photometric depth and stability. Instead, likely because of the poor weather conditions during the two observing runs, the photometric depth of the BOK images turns out to be worse.

5. Conclusions

In Figure 6 the $(U-V)-M_V$ color-magnitude diagram (CMD) of galaxies in Abell 1795 (upper panel, this work) is compared with the same diagram obtained for Abell 754 by McIntosh et al. (2005, lower panel in the figure). For Abell 1795, the colors refer to the 5 kpc apertures and the galaxies reported in the figure are those in common between the WINGS-OPT and BOK catalogs and morphologically classified by Fasano et al. (2012). The U- and V-band magnitudes are taken from the BOK and WINGS-OPT catalogs, respectively. The red and green dots in the plot respectively represent the elliptical and S0 galaxies spectroscopically confirmed members of the cluster.

In spite of the uncertain data quality of the BOK imaging, the red sequence of the A1795 cluster members turns out to be very well defined. The two very blue S0 galaxies in the plot have been visually inspected on the images. One of them turned out to be a close merger, the other one being very close to a bright star. Instead, the elliptical galaxy below the red sequence turns out to be undisturbed, but it is quite small (dwarf-like).

For Abell 754, the colors in the CMD refer to an aperture of 3.34 kpc and the straight line in the plot corresponds to the best fit parameters given for this cluster in Table 8 of McIntosh et al. (2005, last row). The same straight line is also reported in the upper panel of Figure 6. Although the CMDs are obtained with different apertures and for different clusters, the agreement of the two CMDs is quite satisfactory, thus making us confident about the good quality of our U-band photometry.

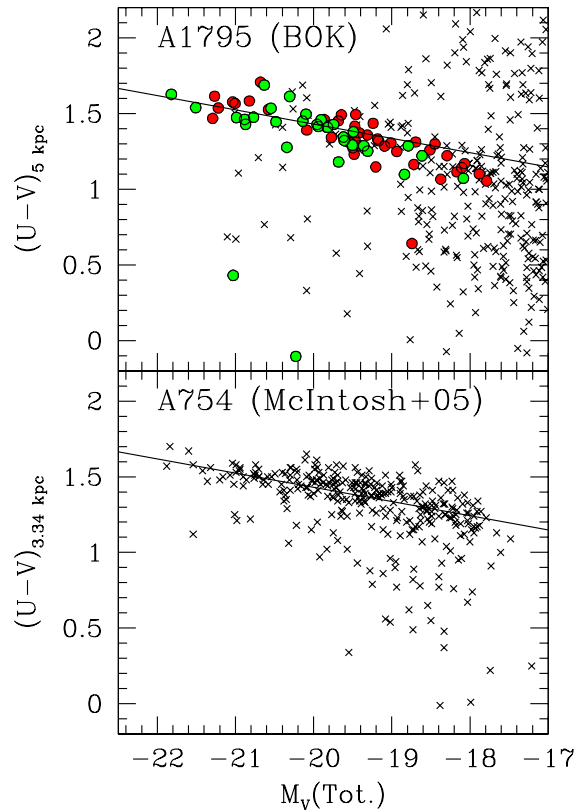


Fig. 6. The color-magnitude diagram $(U-V)-M_V$ for Abell 1795 (this work) and for Abell 754 (McIntosh et al. 2005). The straight lines in the plots correspond to the best fit parameters given for Abell 754 in Table 8 of (McIntosh et al. 2005), last row. The red and green dots in the upper panel, respectively mark elliptical and S0 galaxies that are spectroscopically confirmed members of the cluster Abell 1795.

In a following paper of the series we will present and analyse the color-magnitude diagrams and the average color as a function of both the cluster-centric distance and the morphological type for all clusters belonging to the present sample and for the clusters included in our ongoing OmegaCam@VST survey (6 clusters already imaged in the U-band). Moreover, both sets of data will be used to validate the star formation rates and histories already obtained for WINGS galaxies (Fritz et al. 2011) and to study the color map of individual galaxies at different distances and position angles with respect to the cluster center. This will help to discriminate between the various physical processes possibly responsible of the gas depletion in galaxies infalling into the clusters.

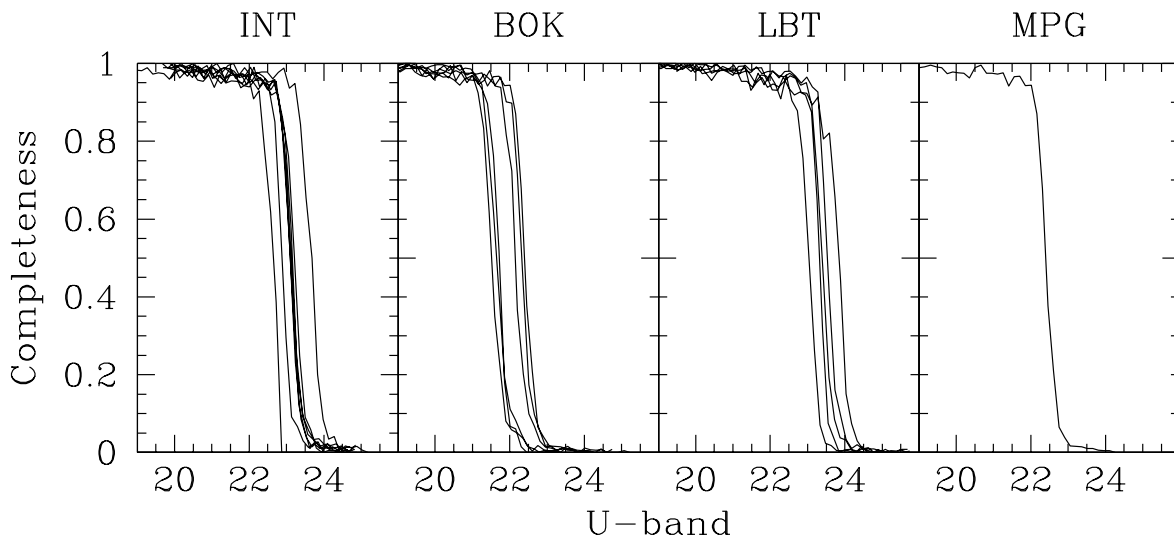


Fig. 5. Fractions of retrieved simulated galaxies as a function of the U-band total magnitudes for the four cameras.

Acknowledgements. We acknowledge partial financial support by contract PRIN/MIUR 2009: “Dynamics and Stellar Populations of Superdense Galaxies” (Code: 2009L2J4MN) and by INAF/PRIN 2011: “Galaxy Evolution with the VLT Survey Telescope (VST)”.

References

- Abazajian, K. et al. 2008, *ApJSupp*, 182, 543
 Abell, G. O. 1958, *ApJS*, 3, 211
 Abraham, R. G. et al. 1996, *ApJ*, 471, 694
 Balogh, M., Morris, S., Yee, H., Carlberg, R., & Ellingson, E. 1997, *ApJ*, 488, L75
 Barbaro, G. and Poggianti, B. M. 1997, *A&A*, 324, 490
 Bertin, E., 2007, SCAMP v 1.3.5 Users guide
 Bertin, E. and Arnouts, S. 1996, *A&AS*, 117, 393
 Blakeslee, et al. 2003, *ApJ*, 596, L143
 Cava, A., Bettoni, D., Poggianti, B. M., Couch, W. J., Moles, M., et al. 2009, *A&A*, 495, 707
 Couch, W., Barger, A., Smail, I., Ellis, R., & Sharples, R. 1998, *ApJ*, 497, 188
 Couch, W., et al. 2001, *ApJ*, 549, 820
 De Lucia, G. et al. 2004, *ApJ*, 610, L77
 Desai, V. et al. 2004, *MNRAS*, 351, 265
 Dressler, A., Oemler, A. J., Couch, W., et al. 1997 *ApJ* 490, 577
 Dressler, A., Smail, I., Poggianti, B., et al. 1999 *ApJS*, 122, 51
 Ebeling, H., Voges, W., Bohringer, H., et al. 1996, *MNRAS*, 281, 799
 Ebeling, H., Edge, A. C., Bohringer, H., et al. 1998, *MNRAS*, 301, 881
 Ebeling, H., Edge, A. C., Allen, S. W., et al. 2000, *MNRAS*, 318, 333
 Ellingson, E. et al. 2001, *ApJ*, 547, 609
 Fasano, G. et al. 2000, *ApJ*, 542, 673
 Fasano, G. et al. 2006, *A&A*, 445, 805
 Fasano, G. et al. 2012, *MNRAS*, 420, 926
 Fritz, J. et al. 2011, *A&A*, 526, 45
 Fukugita, M., Ichikawa, T., Gunn, J. et al. 1996, *AJ*, 111, 1748
 Galadi-Enriquez, D., Trullols, E., Jordi, C. 2000, *A&AS*, 146, 169
 Giallongo, E. e. et al. 2008, *A&A*, 482, 349
 Gladders, M. D. and Yee, H. K. C. 2005, *ApJS*, 157, 1
 Gomez, P. L. et al. 2003, *ApJ*, 584, 210
 Grado, A., Capaccioli, M., Limatola, L., Getman, F. 2010, *MmSait*, 15, 450
 Jordi, K., Grebel, E. K., and Ammon, K. 2006, *A&A*, 460, 339
 Halliday, C. et al. 2004, *A&A*, 427, 397
 Kennicutt, R. C. 1998, *ApJ*, 498, 541
 Kodama, T. et al. 2001, *ApJ*, 562, L9
 Kodama, T. and Bower, R. 2003, *MNRAS*, 346, 1
 Kodama, T. et al. 2004, *MNRAS*, 354, 1103
 Landolt, A. U. 1992, *AJ*, 104, 372
 Lewis, I., Balogh, M., De Propris, R., et al. 2002, *MNRAS*, 334, 673
 Lupton, R. H. 2005, <https://www.sdss3.org/dr8/algorithms/sdssUBVRITransform.php>
 Marmo, C. 2003, PhD thesis, Padova
 McIntosh, D. H. et al. 2004, *ApJ*, 610, 161
 McIntosh, D. H., Zabludoff, A. L., Rix, H.-W., & Caldwell, N. 2005, *ApJ*, 619, 193
 Pignatelli, E. et al. 2006, *A&A*, 446, 373
 Pimblet, K. A. et al. 2002, *MNRAS*, 331, 333
 Poggianti, B. M., Smail, I., Dressler, A., et al., 1999, *AJ*, 518, 576
 Poggianti, B. M. et al. 2004, *ApJ*, 601, 197
 Radovich, M. et al. 2004, *A&A*, 417, 51
 Solanes, J. M. et al. 2001, *ApJ*, 548, 97
 Speziali, R. et al. 2008, *SPIE*, 7014, 70144T
 Stetson, P. B. 1987, *PASP* 99, 191
 Stetson, P. B. 1987, *BAAS* 19, 745
 Stetson, P. B. 1994, Photometry with a Variable PSF, Proceedings of the Workshop held in Quebec City, P.Q., Canada, p.72
 Stetson, P. B. 2000, *PASP* 112, 925
 Stone, R. C. 1997, *AJ*, 114, 2811
 Treu, T. et al. 2003, *ApJ*, 591, 53
 Valentinuzzi, T., Woods, D., Fasano, G., Riello, M., D’Onofrio, M., et al., 2009, *A&A*, 501, 851
 Varela J. et al. 2009, *A&A*, 497, 667.